Quantitative Analysis of Phase Transformation in Ni-Ti Shape Memory Alloys

M. Kimiecik*, J.W. Jones, FASM**, and S. Daly*
University of Michigan
Ann Arbor, Mich.

Transformation heterogeneity in SMAs at the microstructural length scale is characterized by combining SEM and DIC, and correlating the resulting displacement fields to the material microstructure obtained by EBSD.

Digital image correlation (DIC) is a noncontact technique used to track full-field displacements on the surface of an object during mechanical testing. Optical DIC was originally developed in the 1980s and has been improved to the point where commercial software is available to track three-dimensional surface displacements with sub-pixel accuracy[1-3]. Tracking is typically aided by applying a random speckle pattern to the sample surface.

The DIC technique has recently been extended to scanning electron microscopy (SEM-DIC)[4-6], enabling measurement of displacements on the order of nanometers. As DIC was originally developed for use with traditional optical imaging, well-developed techniques exist to remove spatial distortions caused by typical optical imaging elements. However, applying DIC to scanning electron images requires consideration of the more complex distortions created by rastering of the electron beam, the time-dependent nature of image capture, the complex geometry of electron-focusing lenses, and other factors such as electron beam drift over the course of an *in situ* test. If these distortions are correctly accounted for, sub-pixel resolution on the order of that achieved in traditional optical DIC systems is achievable. Because DIC is inherently length scale independent, this means that the capture of strain distributions at very high spatial resolutions is possible.

We are currently developing approaches for using SEM-DIC in conjunction with SEM thermomechanical loading to examine *in situ* microstructure-level deformation in a wide range of materials, geometries, and loading conditions. This article describes how this approach is being used to investigate the complex heterogeneous phase transformation associated with deformation in shape memory alloys (SMAs), which are being used increasingly in high-performance devices and systems. A more detailed description of the approach can be found in Ref. 7. A brief overview of martensitic transformation in SMAs is presented, and experimental methods are described for capturing strain distributions, indicative of transformation extent, during tensile loading. Analyses that can be done to further refine the information gained from such experiments are also briefly illustrated.

**Joint Student Member of ASM International*
*** Member of ASM International*

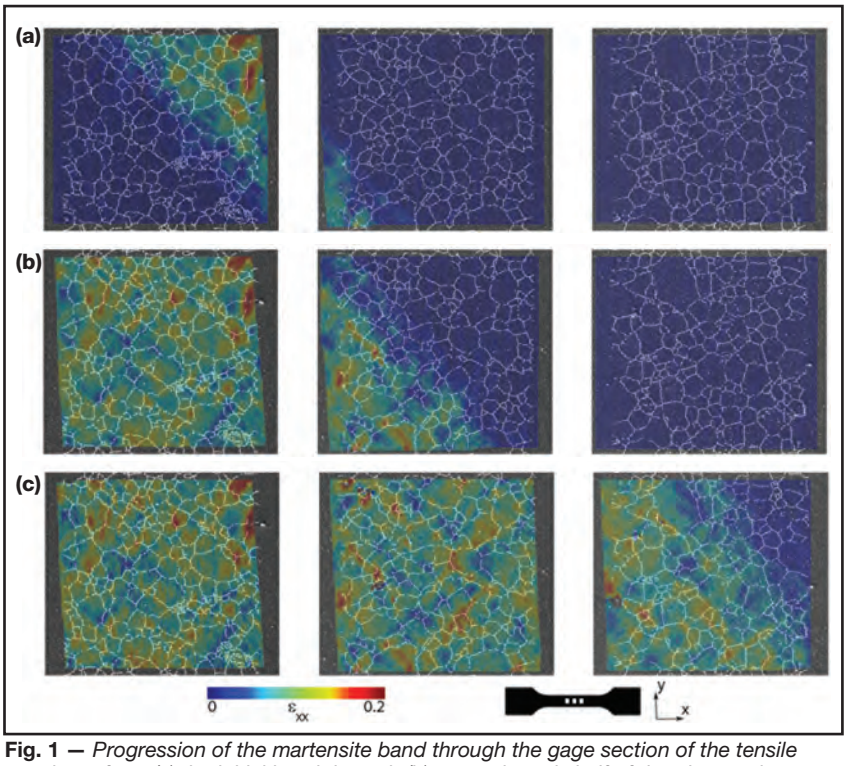

Fig. 1 — *Progression of the martensite band through the gage section of the tensile specimen from (a) the initial band through (b) approximately half of the observed area transformed to (c) nearly complete transformation of the observed area.*

Characterizing SMAs

SMAs are metallic alloys that have unique properties, namely the shape memory effect and superelasticity, which make them well-suited for use in a variety of advanced applications[8]. Both of these properties arise from a solid-to-solid, diffusionless phase transformation between a high-symmetry austenite phase and one or more symmetry-related variants of a martensite phase. In polycrystalline SMAs, the role of microstructure on this phase transformation is critical to SMA function, but the interactions between microstructure and transformation are not well understood. Theoretically, the lath structure of martensite variants developed within a polycrystalline austenite matrix is extremely complex in both superelastic and shape-memory cases. These multivariant configurations have been modeled extensively[9], but it is difficult to confirm these fine microstructures experimentally, leaving fundamental questions about the nature small scale transformation unanswered.

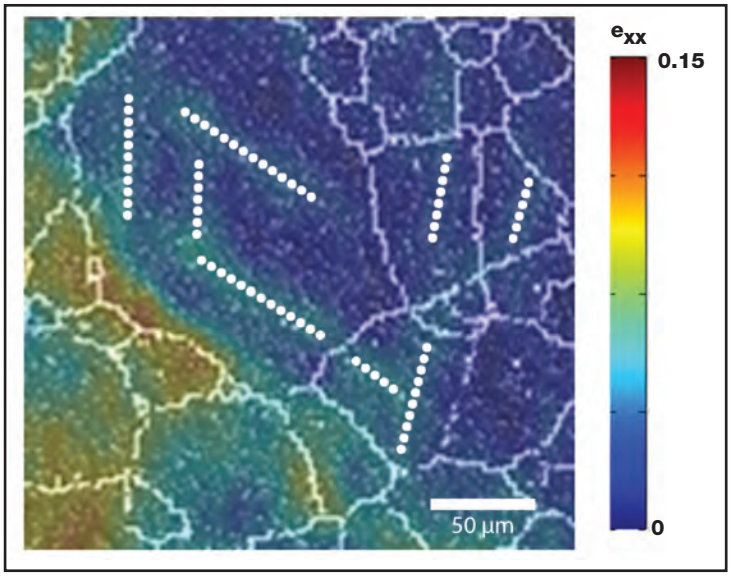

Fig. 2 — *Traces of heterogeneous strain accommodation within grains at the edge of the martensite band. Each dotted white line matches the traces of habit planes associated with type II-2 twinning (0.2152 0.4044 0.8889) <0.7633 0.4981 -0.4114> to within less than 1° error.*

Research has been conducted to characterize the heterogeneity involved with the martensitic transformation at the macroscopic length scale[10], but there is less research to characterize transformation at length scales on the order of grain size or smaller. Previous experiments show that at the macroscale, Lüders-like band structures of localized martensite nucleate and propagate to accommodate strain during tensile loading at relatively low strain rates[11–15]. These martensite bands were previously regarded as monolithic structures composed purely of favorable martensite variants with a sharp transition (defined by a crystallographic habit plane) between the transformed and untransformed regions.

Recent investigations show that the bands are not monolithic, nor do they comprise solely of favorable martensitic variants[16,17]. Rather, the martensite band at the microscale consists of a complex array of interacting variants, and has no clearly defined boundary with untransformed material. Martensite transforms at microstructural length scales in advance of the macroscopic front, and areas within the martensitic band can remain in the parent austenite structure despite massive transformation in surrounding areas. These observations are qualitative in describing martensite formation within a polycrystalline structure. High-resolution, full-field measurement of accommodated strains in austenite, martensite, and two-phase regions over a representative polycrystalline structure can both aid in validating and refining micromechanics-based constitutive models and provide an increased understanding of fundamental deformation mechanisms. SEM-DIC, when combined with local crystal characterization from electron backscatter diffraction (EBSD), provides exactly the type of information needed to accomplish this.

Sample preparation and testing

Tensile specimens were prepared per ASTM E345 from 0.480-mm thick superelastic Ni-Ti (50.8 at% Ni) supplied by Nitinol Devices & Components Inc., Fremont, Calif Specimen tensile axes were oriented parallel to the sheet-rolling direction. Specimens with nominal gage dimensions of 4.5 mm × 18 mm were encapsulated in quartz and backfilled with argon (0.9999 purity). Specimens were heat treated at 900°C for 1 hour and water quenched, resulting in a mean grain diameter of ~70 µm. The microstructure of mechanically ground and polished specimens was characterized by EBSD. Samples were patterned for SEM–DIC using a custom-built apparatus modeled after Ref. 18. In-situ tensile tests were performed on samples loaded under displacement control at a nominal strain rate of 5×10^{-5} s^{-1}. Images of the patterned surface were captured periodically and concurrently with grip displacement and load cell data. High-resolution, quantitative strain fields were calculated using displacements generated by the SEM–DIC procedure[4–6] (Fig. 1a–c). EBSD crystallographic data was aligned with the SEM–DIC measured strain field using platinum markers deposited via focused ion beam.

Test results

SEM–DIC was used to track the evolution of strain in both austenite and martensite phases as martensite bands progressed through the polycrystalline microstructure. At a globally applied stress of ~450 MPa, a single macroscopic martensite band nucleated near the center of the specimen and propagated though the gage section under a nominally constant stress of 400 MPa. Microscale strain maps calculated from SEM–DIC show the progression of the single martensite band (Fig. 1a–c). At the microstructural length scale, the fronts of this band were diffuse and formed a crosshatch-like structure in advance of either side of the stable band (stability is defined as <0.25% change in local strain value from the previous measurement). The diffuse transformation region extended ~150 µm beyond the stable region of the band.

As the front progressed, areas that transformed in the diffuse band first attained the highest local strains when transformation in those areas saturated. Strain accumulation in a particular region ceased after it was subsumed by the stable macroscopic band. Local strain levels remained nominally constant with continued loading, and the macroscopic band propagated past the region.

Average strain values inside the macroscopic martensite band show that complete transformation accommodated 10% average longitudinal strain. However, it is apparent from the spatially resolved strain maps that this strain is accommodated heterogeneously throughout the microstructure. Strains in some subgrain areas were as high as 20%, while others regions experienced no detectable strain despite large amounts

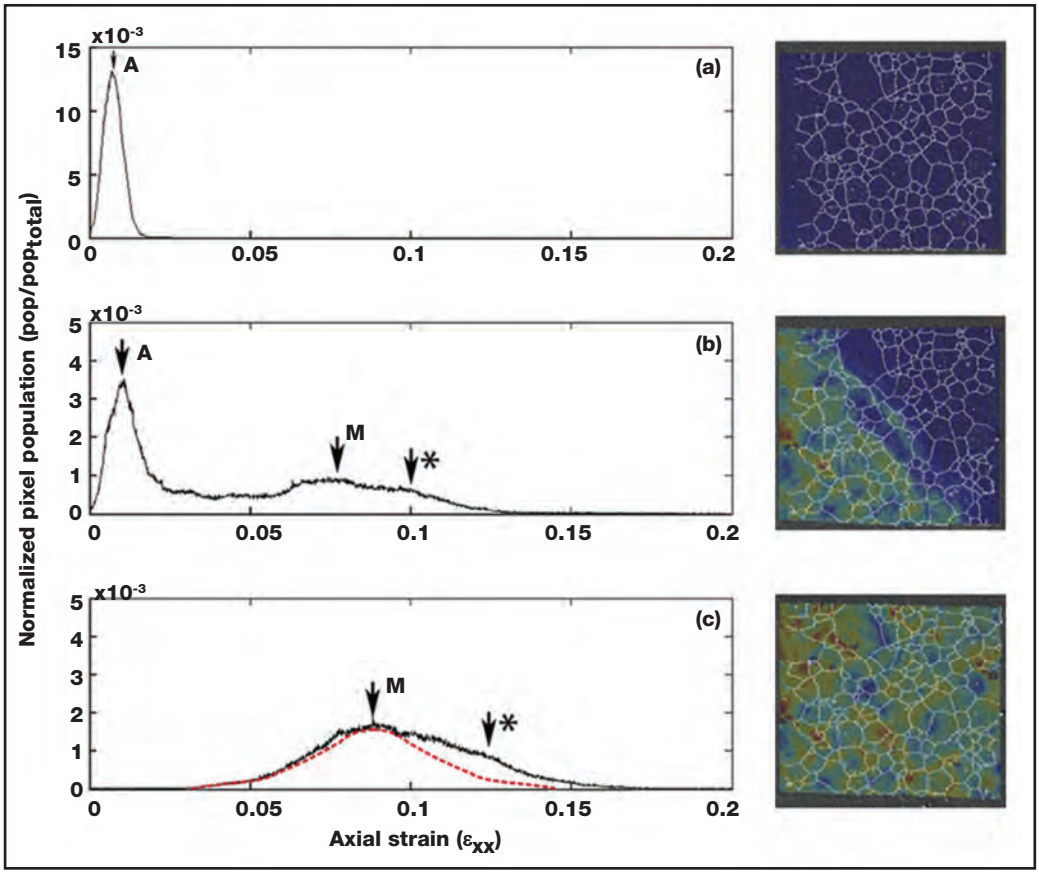

Fig. 3 — *Pixel population of the right area of interest from Fig. 1 binned by their measured strain values. From top to bottom, region progresses from untransformed (a) to half-transformed (b) to fully transformed (c). Arrows indicate peaks corresponding to elastically deformed austenite (A), transformed martensite (M), and an additional high strain deformation mode in the martensite band (*). Symmetric distribution centered around representative martensite strain is outlined in red (c) to highlight deviation from a Gaussian distribution caused by additional high strain deformation.*

of transformation in surrounding regions.

Comparison of strain data to the EBSD map of grain boundaries indicates that areas with larger strains developed primarily along grain boundaries while grain interiors generally experienced lower strain. Because the larger strains are associated with microstructural barriers to dislocation motion (i.e., grain boundaries), it is reasonable to hypothesize that they are caused primarily by additional plastic deformation either within, or closely associated with, martensite transformation.

An example of the usefulness of higher resolution provided by SEM-DIC can be seen in Fig. 2, where the orientations of narrow bands with slightly higher strain are delineated. In most cases, orientations of these regions can be matched with the orientations of type II-2 twin habit planes[19] in the respective grains to within less than 1° deviation. This provides a clear indication that type II-2 twinning is a predominant martensite configuration under these loading conditions.

High-resolution deformation maps created from the SEM-DIC process yield data equivalent to over 80,000 submicron strain gages distributed across each area of interest. Image analysis provides insight into the spatial heterogeneities of deformation, but spatial consideration of strain does not completely explain whether strains are the result of single deformation mode, or multiple deformation modes operating simultaneously (or sequentially) in the microstructural neighborhood.

It is possible to examine the evolution of strain distribution to gain insight into the relative activity of deformation mechanisms (Fig. 3). A single Gaussian distribution centered at approximately 1% strain indicates a single phase of primarily elastically deformed austenite (Fig. 3a). This strain distribution transitions to a martensite peak centered at 6–7% and a higher strain peak that likely represents plastic deformation as the macroscopic martensite band progresses across the field of view (Fig. 3b). When the macroscopic martensite band passes through the field of view, the strain distribution continues to show a an 8% peak associated with saturated martensite, as well as secondary peaks at higher strain levels (Fig. 3c). Secondary peaks have lower intensity than the primary martensite peak, and extend the strain distribution of the saturated band into ranges beyond those for martensitic transformation alone. High-strain deviations could likely represent plastic deformation of transformed martensite, given the previous observations of grain boundary strain concentrations and the annealed state of the sample.

It is still unclear at this point how the plastic deformation implicated by deviation in the strain distribution is interacting with the particular martensite variants that were active during this experiment. Further studies leveraging the infinite scalability of SEM–DIC to smaller length scales and higher resolution are underway to investigate in greater detail the mechanisms responsible for the hetero-

geneous microstructural deformation observed in Ni-Ti shape memory alloys.

Acknowledgment: The authors gratefully acknowledge the financial support of the U.S. Department of Energy, Office of Basic Energy Sciences (Contract No. DE-SC0003996 monitored by Dr. John Vetrano), Mr. Adam Kammers for his development of the SEM–DIC methodology used in this work, and Mr. Jared Tracy for his experimental assistance.

References

1. H.Schreier, J.J. Orteu, and M.A. Sutton, Image correlation for shape, motion and deformation measurements, Springer, Boston, Mass., 2009.
2. Q. Tian and M.N. Huhns, *Computer Vision, Graphics, and Image Process*, 35:220, 1986.
3. M.A. Sutton, et al., *Meas. Sci. Technol.*, 17:2613, 2006.
4. M.A. Sutton, et al., *Exp. Mech.*, 47:775, 2007.
5. M.A. Sutton, et al., *Exp. Mech.*, 47:789, 2007.
6. A. Kammers and S. Daly, Digital image correlation under scanning electron microscopy: experimental methodology and validation (preprint available).
7. M. Kimiecik, J.W. Jones, and S. Daly, *Mat. Lett.*, 95:25, 2013.
8. K. Bhattacharya, Microstructure of martensite: Why it forms and how it gives rise to the shape memory effect; Oxford University Press Inc., N.Y., 2003.
9. D.C. Lagoudas, et al., *Mech. Mater.*, 38:430, 2006.
10. K. Otsuka and X. Ren, *Prog. Mater. Sci.*, 50:511, 2005.
11. J. Shaw and S. Kyriakides, *J. Mech. Phys. Solids*, 43:1234, 1995.
12. J. Shaw and S. Kyriakides, *Acta Mater.*, 45:683, 1997.
13. K. Kim and S. Daly, *Exp. Mech.*, 51:641, 2010.
14. J. Lackmann, et al., *Mater. Charact.*, 62:298, 2011.
15. S. Daly, G. Ravichandran, and K. Bhattacharya, *Acta Mater.*, 55:3593, 2007.
16. L. Brinson, *J. Mech. Phys. Solids*, 52:1549, 2004.
17. S.C. Mao, et al., *Acta Mater.*, 58:3357, 2010.
18. K.N. Jonnalagadda, et al., *Exp. Mech.*, 50:25, 2009.
19. X. Zhang and H. Sehitoglu, *Mat. Sci. Eng. A*, 374:292, 2004.

For more information: Michael Kimiecik, Dept. of Materials Science and Engineering, University of Michigan, Ann Arbor, MI 48109; tel: 734/615-5163; email: mkimieci@umich.edu; www.umich.edu.